applied sciences

MDPI

Article

Effects of Buffer and Capping Layers on Thermal Stability of CoFeB/MgO Frames at Various Temperatures

Byeongwoo Kang [1,†], Young Hyun Hwang [1,†], Yong Jin Kim [1,2], Jong Seong Lee [1], Seo Hyun Song [1], Seungwon Lee [1], Jisung Lee [3], OukJae Lee [2], Seung-Young Park [3,*] and Byeong-Kwon Ju [1,*]

1 Display and Nanosensor Laboratory, Department of Electrical Engineering, Korea University, Seoul 02841, Republic of Korea; kang7369@korea.ac.kr (B.K.)
2 Center for Spintronics, Korea Institute of Science and Technology, Seoul 02792, Republic of Korea
3 Center for Scientific Instrumentation, Korea Basic Science Institute, Daejeon 34133, Republic of Korea
* Correspondence: parksy@kbsi.re.kr (S.-Y.P.); bkju@korea.ac.kr (B.-K.J.)
† These authors contributed equally to this work.

Abstract: The utilization of CoFeB thin films in spintronic devices has attracted significant attention due to their exceptional magnetic properties, which include high saturation magnetization and spin polarization. However, the effect of ambient temperature on the magnetic properties of CoFeB/MgO frames, particularly those with different buffer and capping layers, remains unexplored. Therefore, in this study, the magnetostatic and dynamic properties of CoFeB/MgO frames were investigated at various temperatures. Using vibrating sample magnetometry and ferromagnetic resonance spectroscopy, changes in key parameters such as saturation magnetization, the Gilbert damping constant, magnetic anisotropy field, in-plane uniaxial magnetic anisotropy energy, and thermal stability factor were investigated. Furthermore, the thermal stabilities of CoFeB/MgO frames with Ta buffer and capping layers were compared with those of CoFeB/MgO frames with W buffer and capping layers by examining the changes in the key parameters at various temperatures. These results reveal that the thermal stability of the latter surpassed that of the former. This study provides significant insights for the development of thermally robust spintronic devices capable of operating above room temperature.

Keywords: high-temperature measurements; vibrating sample magnetometry; ferromagnetic resonance; spintronics; magnetic thin film; CoFeB thin film

check for updates

Citation: Kang, B.; Hwang, Y.H.; Kim, Y.J.; Lee, J.S.; Song, S.H.; Lee, S.; Lee, J.; Lee, O.; Park, S.-Y.; Ju, B.-K. Effects of Buffer and Capping Layers on Thermal Stability of CoFeB/MgO Frames at Various Temperatures. *Appl. Sci.* **2024**, *14*, 2394. https://doi.org/10.3390/app14062394

Academic Editors: R. Raudel Peña-Garcia and Yuset Guerra Dávila

Received: 8 February 2024
Revised: 4 March 2024
Accepted: 5 March 2024
Published: 12 March 2024

1. Introduction

Recently, extensive research has been conducted on CoFeB thin films, which are characterized by low Gilbert damping constant (α) and high spin polarization [1–6]. Their exceptional magnetic properties, which include high saturation magnetization and spin polarization, has resulted in the emergence of spin-transfer torque magnetic random-access memory (STT-MRAM) and spin-orbit torque magnetic random-access memory (SOT-MRAM) devices [7–11]. These devices feature a magnetic tunnel junction (MTJ) structure that is composed of a thin oxide tunnel layer positioned between two ferromagnetic metal layers [12–14]. Owing to their non-volatility and high-performance information storage characteristics, STT-MRAM and SOT-MRAM have garnered attention as promising candidates for next-generation memory technologies [14,15]. In a MTJ, tunneling electrons are spin-polarized, resulting in a higher tunneling probability when the two ferromagnetic metal layers exhibit an alignment of magnetization directions in a parallel configuration, and a lower probability when they are aligned in an antiparallel configuration. CoFeB thin films, known for their magnetic effects, including giant magnetoresistance (GMR) [16–18], tunneling magnetoresistance (TMR) [19,20], the Hall effect [21,22], and anisotropic magnetoresistance (AMR) [23,24], play a pivotal role in these structures owing to their high saturation magnetization, Curie temperature, and low coercive field, rendering them suitable for use in various spintronic devices [25].

A spintronic device utilizes the spin degree of freedom of an electron to store and transmit information [15], offering advantages such as reduced energy consumption, rapid operation, and high density [26]. MTJs, comprising multiple magnetic and non-magnetic layers, are a prime example of spintronic devices. Although the TMR effect was initially discovered in Fe/Ge/Co-based MTJ structures in 1975, the performance of the MTJ was limited [27]. When (100)-oriented crystalline MgO was used instead of amorphous Al_2O_3 as a tunnel barrier in MTJ, superior interfacial properties and TMR ratios were observed [1]. Subsequently, the introduction of soft CoFeB thin films has considerably broadened the scope of their enhanced performance. Notably, research has revealed that MTJs constructed with a Ta/CoFeB/MgO/CoFeB/Ta structure exhibit a remarkable TMR ratio, of 604%, at room temperature [1,2,28–31]. Furthermore, recent studies have contributed to optimizing MTJ structures by incorporating specific heavy metals, including Ta, Pt, Hf, Mo, Ru, and W, as buffer and capping layers [32–37]. In particular, a CoFeB/MgO frame with W buffer and capping layers demonstrated higher annealing stability compared to a CoFeB/MgO frame with Ta buffer and capping layers [36].

However, only a few reports have examined the effect of high temperature on the magnetic properties of CoFeB thin films with various buffer and capping layers. A few studies have investigated the temperature dependence of magnetic properties in a variety of MTJ and magnetic multi-layer structures, revealing a decrease in thermal stability with increasing temperatures [38–45]. Therefore, analysis of the high-temperature characteristics of magnetic thin films from various perspectives such as materials, interfaces, structures, and annealing conditions is essential. For widespread application of spintronic devices, such as STT-MRAM, across various settings, it is necessary for their characteristics to remain stable across a broad range of operating temperatures. Therefore, it is essential to minimize any fluctuation in the magnetic properties of thin films [43]. Additionally, thermal stability is crucial for increasing the storage capacity of spintronic devices, including MTJs [2,46–51]. Therefore, there is a need to analyze the magnetic properties of CoFeB thin films with different buffer and capping layers under high-temperature conditions.

In this study, we investigated the temperature dependence of the magnetic properties of CoFeB thin films featuring different buffer and capping layers at high temperatures. We measured both the static and dynamic magnetic properties of CoFeB thin films with different buffer and capping layers at high temperatures, and then analyzed their thermal stabilities. Ta/CoFeB/MgO/Ta and W/CoFeB/MgO/W structures with different buffer and capping layers are used and these structures are fabricated via a sputtering process. The impact of the Ta buffer and capping layers as well as that of the W buffer and capping layers on the temperature dependence of the CoFeB thin film was systematically analyzed. We used vibrating sample magnetometry (VSM) for static property analysis and ferromagnetic resonance (FMR) spectroscopy for dynamic property analysis. We conducted measurements at various temperatures above room temperature to derive values for saturation magnetization (M_s), Gilbert damping constant (α), magnetic anisotropy field (H_k), in-plane uniaxial magnetic anisotropy energy (K_u), and thermal stability factor (Δ) as functions of temperature. Our findings suggest these materials have potential applications in the design of magnetic film stacks that are suitable for high-temperature applications in spintronic devices.

2. Materials and Methods

2.1. Fabrication

The samples were prepared via DC/RF magnetron sputtering on thermally oxidized Si layer substrates at room temperature. CoFeB target with 99.9% purity, MgO target with 99.9% purity, Ta target with 99.5% purity, and W target with 99.5% purity were used as sputtering targets. The base pressure of the sputtering chamber was maintained below 5×10^{-8} Torr and the deposition rate was kept below 0.5 Å/s. Deposition rates were determined by measuring the film thickness using atomic force microscopy (AFM). During sputtering, the substrate was rotated to ensure uniform deposition of the films. The prepared samples were rectangular shapes measuring 4 × 4 mm (Figure 1) and consisted of substrate/Ta(3)/CoFeB(7)/MgO(1)/Ta(3) or substrate/W(3)/CoFeB(7)/MgO(1)/W(3) configurations (thickness indicated in nm within parentheses). The composition of the CoFeB alloy sputtering target was Co:Fe:B = 20:60:20 ($Co_{20}Fe_{60}B_{20}$); 3 nm thick Ta and 3 nm thick W served as the buffer layers and MgO(1)/Ta(3) and MgO(1)/W(3) served as the capping layers. The Ar working pressures of MgO, CoFeB, Ta, and W were 4, 1.5, 3, and 3 mTorr, respectively. Following post-annealing at 350 °C for 1 h under vacuum, the temperature-dependent magnetic properties of the samples were measured and analyzed to elucidate the effects of the Ta and W buffer and capping layers on the temperature dependence of the magnetic properties.

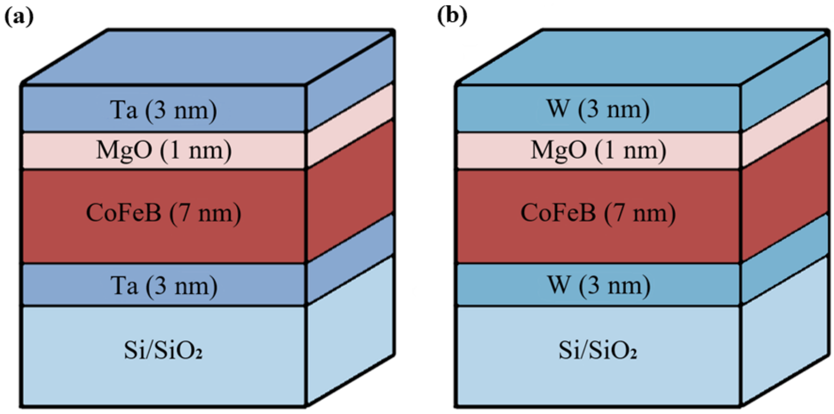

Figure 1. Schematics of the configurations for (**a**) Ta buffer and capping layers sample and (**b**) W buffer and capping layers sample.

2.2. Measurements

We conducted measurements on the samples featuring Ta buffer and capping layers, as well as on those with W buffer and capping layers. We examined the crystalline structures and chemical compositions of the samples with Ta and W buffer and capping layers using X-ray diffractometer (XRD; X'Pert PRO, PANalytical, Almelo, The Netherlands) and X-ray photoelectron spectrometer (XPS; PHI VersaProbe III, ULVAC-PHI, Kanagawa, Japan), respectively. We observed the magnetic properties of each sample by varying the temperature and taking measurements. Diverse magnetic properties were characterized at different temperatures, with the samples analyzed for both static and dynamic magnetic properties. Static magnetic properties, such as M_s, were measured using a VSM (LakeShore 7404, Lake Shore Cryotronics Inc., Westerville, OH, USA). Dynamic magnetic properties, including α, were evaluated in the frequency range of 5–20 GHz using FMR spectroscopy. Both VSM and FMR spectroscopies were performed in the in-plane direction. VSM measurements were conducted at temperatures ranging from room temperature (293 K) to 550 K. Values at temperatures beyond 550 K were determined using the $T^{1/3}$ power law [52], represented as:

$$M_s(T) = M_0 \times \left(1 - \frac{T}{T_{M_s=0}}\right)^{\frac{1}{3}} \tag{1}$$

where M_0 and T represent the M_s values at 0 K and absolute temperature, respectively. To analyze the temperature dependence of α, we performed FMR spectroscopy measurements in the temperature range of 306–443 K using a field-sweep technique and a coplanar waveguide. The frequency range of 5–20 GHz was utilized for the setup. The raw FMR spectra were fitted using the derivative of a Lorentzian line shape to determine the resonance field (H_r) and peak-to-peak linewidth (ΔH_{pp}). We obtained the values of α and H_k from the extracted H_r and ΔH_{pp}.

3. Results and Discussion

3.1. Structural and Chemical Composition Analysis via XRD and XPS

The crystalline structures and chemical compositions of the samples with the Ta and W buffer and capping layers were examined by XRD and XPS, respectively. Figure 2a shows the XRD scans of the samples with the Ta and W buffer and capping layers. Both samples with the Ta and W buffer and capping layers have broad and low peaks, indicating they are in an amorphous state. This is because the B content constrained the nucleation of CoFe, resulting in the absence of crystallization [53]. Figure 2b,c show the XPS depth profiles of the Ta/CoFeB/MgO/Ta and W/CoFeB/MgO/W samples, respectively. The XPS depth profile confirms the presence of B in the CoFeB layer, which explains the amorphous states of both samples.

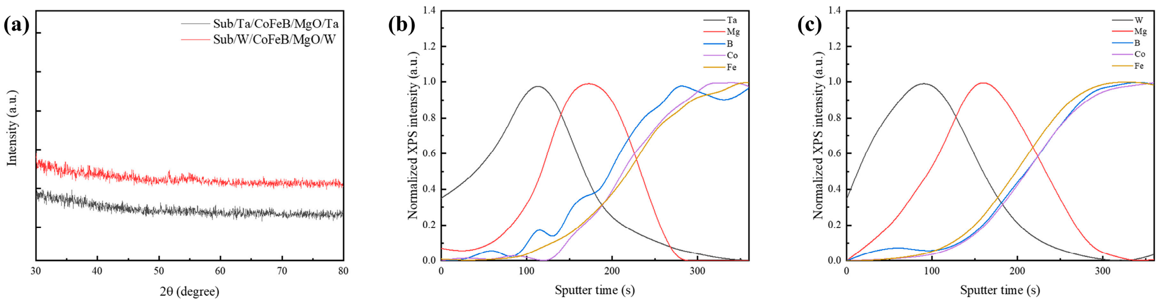

Figure 2. (**a**) X-ray diffractometer (XRD) scans of the samples with Ta and W buffer and capping layers, (**b**) X-ray photoelectron spectrometer (XPS) depth profile of the sample with Ta buffer and capping layers, and (**c**) XPS depth profile of the sample with W buffer and capping layers.

3.2. Static Property Analysis Based on VSM

The magnetic properties of the samples with the Ta and W buffer and capping layers were examined to compare the effects of temperature changes on the magnetostatic properties using a magnetic hysteresis loop (*M*–*H* loop). Magnetic fields (with strengths ranging from +12.5 to −12.5 kOe) were applied in the in-plane direction at four temperatures: room temperature (293 K), 400, 500, and 550 K (Figure 3). Figure 3a,b show the *M*–*H* loops of the Ta/CoFeB/MgO/Ta and W/CoFeB/MgO/W samples, respectively. The low-scale loops are depicted in the insets in Figure 3. The value of M_s was derived from these loops. Both samples exhibited a decrease in M_s with increasing temperature. The M_s values for the samples with the Ta buffer and capping layers were 1133, 1089, 1045, and 1005 emu/cc at 293, 400, 500, and 550 K, respectively, whereas those for samples with W buffer and capping layers were higher at the same temperature (1213, 1163, 1111, and 1065 emu/cc at 293, 400, 500, and 550 K, respectively). This decrease in M_s value with an increase in temperature can be attributed to the increase in thermal fluctuations with temperature [54]. The difference in M_s values between samples with Ta and W buffer and capping layers was imputed to the intermixing between the CoFeB and buffer layers, leading to the formation of a magnetic dead layer and considering the potential influence of intermixing between the Si atoms and layers [55–57].

The $T^{1/3}$ power law was used to fit the M_s values at different temperatures. The results are shown in Figure 4; the data points denote the experimental values and the line represents the fitted values. The choice of the $T^{1/3}$ power law was driven by the large error between the fitting values of Bloch's law and experimental values at high temperatures [43,52,58]. Differences in magnetization values between the samples with Ta and W buffer and capping layers indicated the presence of a magnetic dead layer within the CoFeB layers, attributed to intermixing between the CoFeB and buffer layers [55]. The sample with Ta buffer and capping layers exhibited a lower M_s value than that of the sample with W buffer and capping layers, owing to the greater intermixing between CoFeB and buffer layers in the former sample. Depending on the buffer layer materials, the degree of diffusion of the buffer layer and the influence of the orbital and lattice by the interface vary, and these affect the magnetic dead layer and magnetization change. As a result, the magnetic dead layer in the W/CoFeB sample was thinner compared to that in the Ta/CoFeB sample, resulting in a higher M_s for the W/CoFeB sample [59].

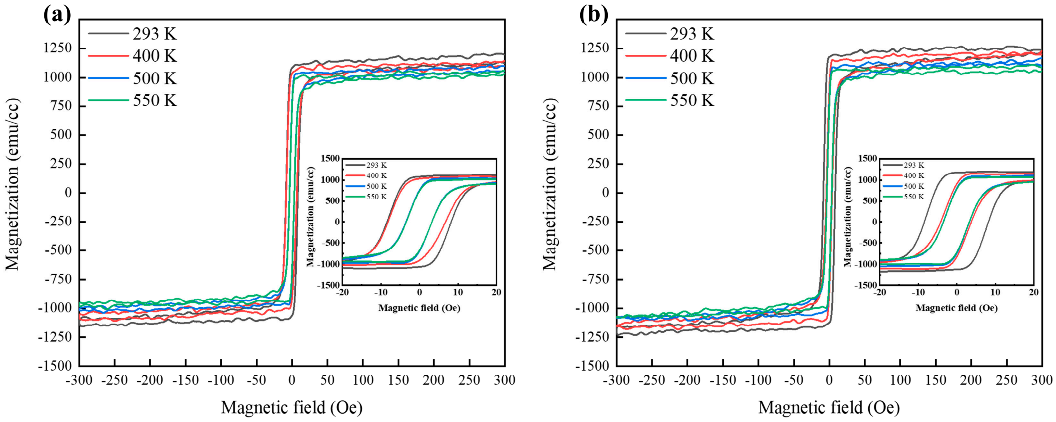

Figure 3. Magnetic hysteresis (*M*–*H*) loops at different temperatures of (**a**) Ta buffer and capping layers sample and (**b**) W buffer and capping layers sample.

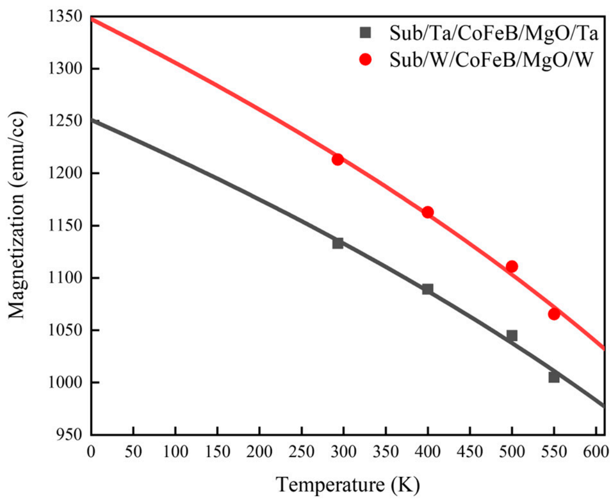

Figure 4. Variation in M_s for samples with Ta and W buffer and capping layers as a function of ambient temperature. Closed symbols denote the experimental data and solid lines correspond to the fitting based on Equation (1).

3.3. Dynamic Property Analysis Based on FMR Spectroscopy

The temperature dependence of α was investigated using FMR spectroscopy to verify the effects of Ta and W buffer and capping layers on the dynamic properties of the CoFeB/MgO frame. Figure 5a,b show the raw FMR spectra and the fitting of the Lorentzian function to extract the linewidth and resonance magnetic field. Black symbols and the red line represent the experimental data and the Lorentzian line shape, respectively. The FMR spectra were measured in the direction of the sample surface and parallel to the external magnetic field. H_r and ΔH_{pp} values were extracted from these spectra.

Figure 5 shows the normalized FMR spectra for convenience in comparing the resonance field and linewidth. Figure 5c,d show the FMR spectra of the W buffer and capping layers sample in the frequency range of 5–20 GHz at 373 K and 403 K, respectively. As the frequency increased, both the resonance field and linewidth increased. Figure 5e shows the normalized FMR spectra of the Ta buffer and capping layers sample at a fixed frequency of f = 19 GHz with increasing temperature. Both the resonance field and linewidth increased with increasing temperature.

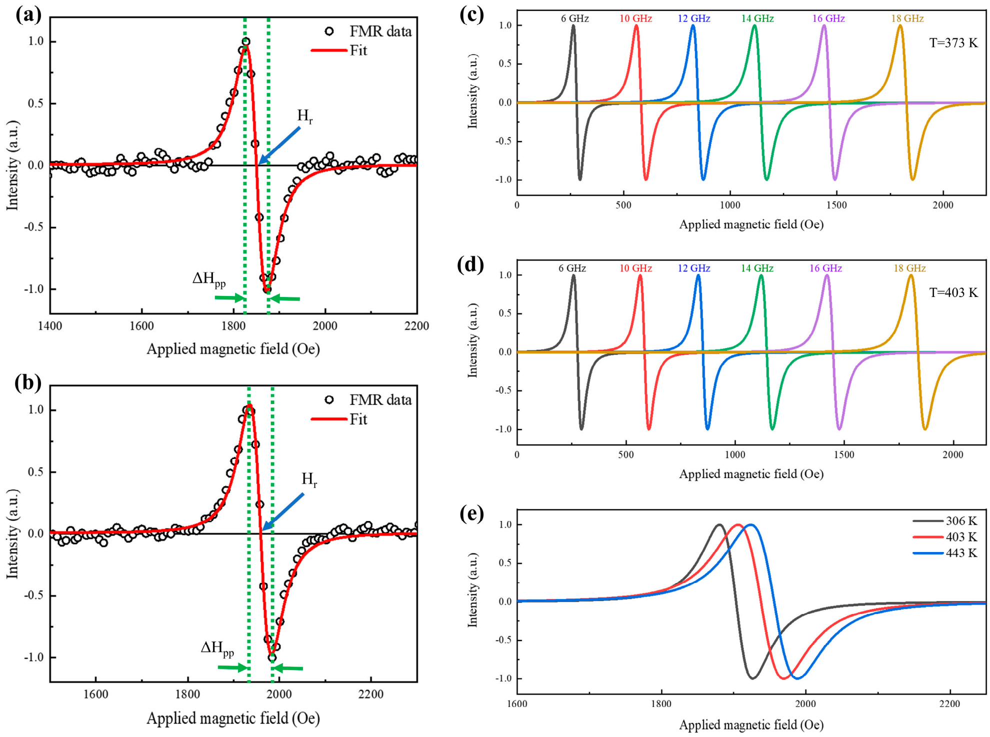

Figure 5. Ferromagnetic resonance (FMR) derivate absorption line (black open symbols) fitted with Lorentzian function (red line) (**a**) at 18 GHz for W buffer and capping layers sample, (**b**) at 19 GHz for Ta buffer and capping layers sample, (**c**) FMR absorption spectra at 373 K for W buffer and capping layers sample with frequency of 5–20 GHz, (**d**) FMR absorption spectra at 403 K for W buffer and capping layers sample with frequency of 5–20 GHz, and (**e**) FMR absorption spectra of Ta buffer and capping layers sample at different temperatures.

We determined the value of α using an expression based on the extracted linewidth [60]:

$$\Delta H_{\mathrm{pp}} = \frac{4\pi\alpha f}{\gamma} + \Delta H_0 \tag{2}$$

where r denotes the gyromagnetic ratio and ΔH_0 represents inhomogeneous linewidth broadening. The term α was determined from the slope of Equation (2), which demonstrates a linear proportionality to frequency. As the frequency increases, the linewidth increases linearly, according to Equation (2), and as the temperature increases, the slope of the fitting line increases. Therefore, we deduced that α exhibits temperature dependence [61–63]. The cause was attributable to the phenomenon of magnetization relaxation, which diminishes with a decrease in temperature [61,62].

Additionally, we measured H_{k} as a function of temperature using the Kittel equation [64]:

$$f = \left(\frac{\gamma}{2\pi}\right)\sqrt{(H_{\mathrm{k}} + H_{\mathrm{r}})(H_{\mathrm{k}} + H_{\mathrm{r}} + 4\pi M_{\mathrm{s}})} \tag{3}$$

As shown in Figure 5c–e, H_{r} increases as the measuring frequency increases at a constant temperature, and similarly, H_{r} increases as the measuring temperature increases at a constant frequency. According to Equation (3), the increase in H_{r} with temperature was attributable to the decrease in M_{s} with an increase in temperature [61].

Figure 6a shows that α for the prepared samples exhibits a temperature dependence. As the ambient temperature increased from 306 to 443 K, the α values for the samples with Ta and W buffer and capping layers increased from 0.0033 to 0.0059 and from 0.0055 to 0.0065, respectively. For all samples, α increased with an increase in temperature, consistent with the typical behavior in ferromagnetic materials owing to electron scattering through interband and/or intraband transitions [65,66]. This increase is attributed to the reduction in electron lifetime at high temperatures [67].

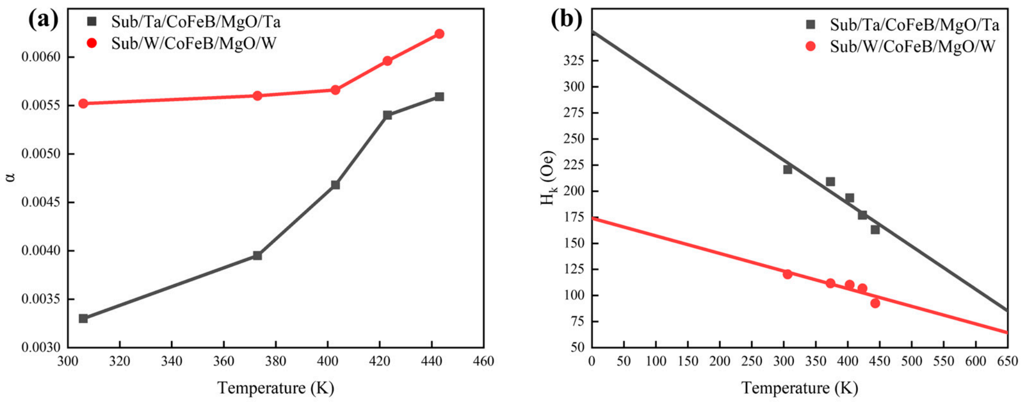

Figure 6. (**a**) Gilbert damping constant of Ta buffer and capping layers sample and W buffer and capping layers sample as a function of temperature. (**b**) Symbols show magnetic anisotropy field measured by FMR between 306 and 443 K for Ta buffer and capping layers sample and W buffer and capping layers sample. Solid lines represent linear fits of experimental data.

These findings highlight that the thermal stability of α was superior for the sample with the W buffer and capping layers compared to the sample with the Ta buffer and capping layers at higher temperatures. At temperatures of 373, 403, 423, and 443 K, α values for the samples with Ta buffer and capping layers increased by approximately 19.7, 41.8, 63.6, and 69.4%, respectively, compared to those at room temperature. In contrast, for the sample with W buffer and capping layers, the increase in α values were 1.4, 2.5, 8.0, and 13.0%, respectively. Consequently, the sample with W buffer and capping layers exhibited higher α values at various temperatures, but showed less significant temperature dependence than the sample with Ta buffer and capping layers. This finding aligns with previous research and may be attributed to differences in interfacial morphologies and spin-mixing conductance [68–70].

Figure 6b shows the temperature dependence of H_k for the prepared samples, measured as a function of temperature and represented by solid symbols. As the ambient temperature increased from 306 to 443 K, H_k values for the samples with Ta and W buffer and capping layers decreased from 220.6 to 163.0 Oe and from 120.3 to 92.4 Oe, respectively. Unlike α, H_k tends to decrease linearly for all samples with an increase in the temperature, as indicated by the solid lines in Figure 6b [43]. In Figure 6b, the data points denote experimental values and the lines represent linear fits to the experimental values. By comparing the slopes of the fitted lines for H_k of the prepared samples, the effects of the Ta and W buffer and capping layers on the temperature dependence of H_k were examined. The slopes of the fitted lines for the Ta and W buffer and capping layers samples were -0.412 and -0.169, respectively. Although H_k for the W buffer and capping layers samples was lower than that for the Ta buffer and capping layers sample, the thermal stability was higher for the W buffer and capping layers sample, consistent with α.

3.4. Thermal Stability Characteristics

To investigate the thermal stability characteristics of CoFeB thin films with Ta and W buffer and capping layers, we extracted M_s and H_k data and calculated K_u and Δ values. The values were analyzed along with the fitted data derived through interpolation based on the experimentally obtained data.

The value of K_u is calculated using Equation (4) [71]:

$$K_u = \frac{M_s H_k}{2} \tag{4}$$

A linear approximation was applied for interpolation to estimate the H_k values at measurable temperatures using FMR spectroscopy. The M_s values were calculated using the $T^{1/3}$ power law. Figure 7a shows the temperature dependence of K_u for both the prepared samples, where the data points represent values determined through experimentally measured data for M_s and H_k, and the solid lines are computed based on the temperature changes in M_s and H_k. As the temperature increased from 293 to 550 K, the K_u values for the samples with Ta and W buffer and capping layers decreased from 1.32×10^5 to 0.64×10^5 erg/cc and from 0.76×10^5 to 0.43×10^5 erg/cc, respectively. In particular, at 400, 500, and 550 K, the K_u values for the sample with Ta buffer and capping layers decreased by 22.1, 41.6, and 51.7%, respectively, compared with those at room temperature. Furthermore, those for the samples with W buffer and capping layers decreased by 18.1, 34.1, and 42.8%, respectively, compared with those at room temperature. These results demonstrated that the sample with Ta buffer and capping layers exhibited a higher K_u value than the sample with W buffer and capping layers. Furthermore, the absolute K_u value of the W buffer and capping layers sample was smaller than that of the Ta buffer and capping layers sample, but the relative thermal stability of K_u for the sample with W buffer and capping layers was higher than that for the sample with Ta buffer and capping layers at high temperatures. Notably, the magnetic anisotropy characteristics of magnetic thin film samples show less dependence on temperature. This is advantageous for the temperature dependence of data read–write operations in memory devices, such as STT-MRAM and SOT-MRAM. Simultaneously, the temperature dependence on the external magnetic field must remain stable with minimal changes. Therefore, it is imperative to analyze the relative temperature dependence of the thermal stability factor.

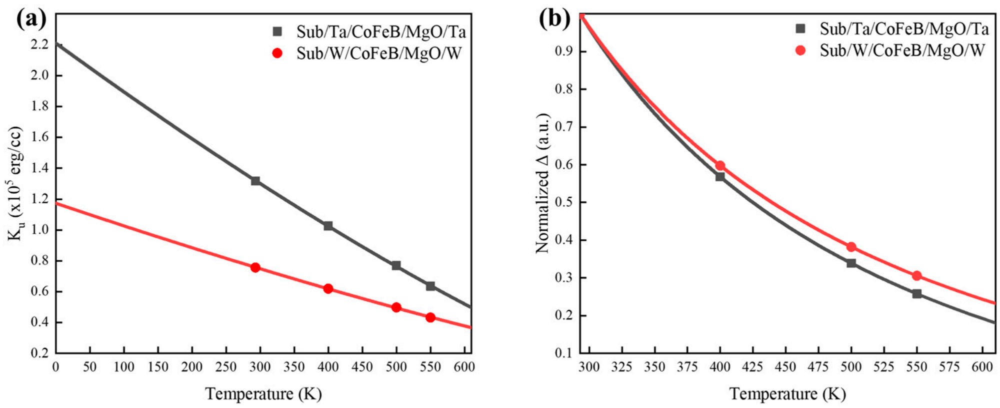

Figure 7. Magnetic properties of Ta buffer and capping layers sample and W buffer and capping layers sample as a function of temperature: (**a**) in-plane uniaxial magnetic anisotropy energy. Closed symbols represent in-plane uniaxial magnetic anisotropy energy derived from experimentally measured data for M_s and H_k, and the solid lines are computed based on the temperature changes in M_s and H_k; (**b**) normalized thermal stability factor. Closed symbols represent normalized thermal stability factor derived from experimentally measured data for M_s and H_k, and the solid lines are computed based on the temperature changes in M_s and H_k.

The thermal stability factor is calculated as [72,73]:

$$\Delta = \frac{K_u V}{k_B T} \tag{5}$$

where V and T represent the volume of the magnetic film layer and absolute temperature, respectively. To compare the relative changes in the thermal stability factor between the Ta buffer and capping layers and W buffer and capping layers at various temperatures, these values were normalized at 293 K. Figure 7b shows the temperature dependence of Δ for both the prepared samples, where the data points denote values determined from experimentally measured data for M_s and H_k, and the solid lines are computed based on the temperature changes in M_s and H_k. The temperature-dependent changes in the thermal stability factor show that the samples with Ta buffer and capping layers decreased by 43.2, 66.1, and 74.2% at 400, 500, and 550 K, respectively, compared with room temperature. Furthermore, those of the samples with W buffer and capping layers decreased by 40.3, 61.8, and 69.4% at 400, 500, and 550 K, respectively. These results indicate that the sample with Ta buffer and capping layers exhibited a larger temperature-dependent change in the thermal stability factor compared to sample with W buffer and capping layers. The normalized thermal stability factor enables a comparison of the thermal stability factors at various temperatures. In conclusion, the thermal stability factor of the samples with W buffer and capping layers was less sensitive to temperature compared with that of the sample with Ta buffer and capping layers.

4. Conclusions

In this study, we explored the use of CoFeB thin films in high-temperature applications, such as in the automotive industry, by investigating the variations in their magnetic properties at high temperatures. We examined the temperature dependence of the magnetization properties (M_s, α, H_k, K_u, and Δ) of the Ta/CoFeB/MgO/Ta and W/CoFeB/MgO/W structures at temperatures exceeding room temperature. Both static and dynamic properties were analyzed to compare the temperature-dependent characteristics of the samples with Ta buffer and capping layers and samples with W buffer and capping layers. Our results revealed that the values of M_s, H_k, K_u, and Δ decreased with an increase in temperature for both samples, whereas the values of α increased. We evaluated the thermal stability of the two samples by combining the results of VSM and FMR spectroscopy obtained at high temperatures. The α value of the sample with Ta buffer and capping layers increased by 69.4% at 443 K compared with that at 293 K, whereas that of the sample with W buffer and capping layers increased by 13%. The Δ value of the sample with Ta buffer and capping layers decreased by 74.2% at 550 K compared with that at 293 K, whereas that of the sample with W buffer and capping layers decreased by 69.4%. These results underscored that the sample with W buffer and capping layers exhibited less variation in α and Δ values with temperature than the sample with Ta buffer and capping layers. The findings of this study provide significant insights for the development of thermally robust spintronic devices that can operate at high temperatures.

Author Contributions: Conceptualization, B.K. and Y.H.H.; methodology, B.K., Y.J.K., J.L. and O.L.; formal analysis, B.K. and J.S.L.; investigation, B.K., S.L. and S.H.S.; resources, S.-Y.P. and B.-K.J.; data curation, Y.H.H.; writing—original draft preparation, B.K.; writing—review and editing, B.K. and Y.H.H.; supervision, S.-Y.P. and B.-K.J.; funding acquisition, B.-K.J. All authors have read and agreed to the published version of the manuscript.

Funding: This research received no external funding.

Institutional Review Board Statement: Not applicable.

Informed Consent Statement: Not applicable.

Data Availability Statement: Data are contained within the article.

Acknowledgments: This work was supported by the Brain Korea 21 Plus Project in 2023, Samsung Electronics Co., Ltd. (IO201214-08159-01), KIST Institutional Program and Institute for information & communications Technology Promotion (IITP) grant funded by the Korea government (MSIP) (No. 2022-0-01026), Commercialization Promotion Agency for R&D Outcomes(COMPA) funded by the Ministry of Science and ICT (MSIT) (1711198544, Development of analytical instrumentation for electromagnetics/optics/thermal characteristics under extreme environment), and Korea Institute for Advancement of Technology (KIAT) grant funded by the South Korean government (MOTIE) (P0020967, Advanced Training Program for Smart Sensor Engineers).

Conflicts of Interest: The authors declare no conflicts of interest.

References

1. Parkin, S.S.; Kaiser, C.; Panchula, A.; Rice, P.M.; Hughes, B.; Samant, M.; Yang, S.-H. Giant tunnelling magnetoresistance at room temperature with MgO (100) tunnel barriers. *Nat. Mater.* **2004**, *3*, 862–867. [CrossRef]
2. Ikeda, S.; Miura, K.; Yamamoto, H.; Mizunuma, K.; Gan, H.; Endo, M.; Kanai, S.; Hayakawa, J.; Matsukura, F.; Ohno, H. A perpendicular-anisotropy CoFeB–MgO magnetic tunnel junction. *Nat. Mater.* **2010**, *9*, 721–724. [CrossRef] [PubMed]
3. Yu, H.; Huber, R.; Schwarze, T.; Brandl, F.; Rapp, T.; Berberich, P.; Duerr, G.; Grundler, D. High propagating velocity of spin waves and temperature dependent damping in a CoFeB thin film. *Appl. Phys. Lett.* **2012**, *100*, 262412. [CrossRef]
4. Li, M.; Lu, J.; Akyol, M.; Chen, X.; Shi, H.; Han, G.; Shi, T.; Yu, G.; Ekicibil, A.; Kioussis, N.; et al. The impact of Hf layer thickness on the perpendicular magnetic anisotropy in Hf/CoFeB/MgO/Ta films. *J. Alloys Compd.* **2017**, *694*, 76–81. [CrossRef]
5. Zhang, Y.; Fan, X.; Wang, W.; Kou, X.; Cao, R.; Chen, X.; Ni, C.; Pan, L.; Xiao, J.Q. Study and tailoring spin dynamic properties of CoFeB during rapid thermal annealing. *Appl. Phys. Lett.* **2011**, *98*, 042506. [CrossRef]
6. Chen, S.; Tang, M.; Zhang, Z.; Ma, B.; Lou, S.; Jin, Q. Interfacial effect on the ferromagnetic damping of CoFeB thin films with different under-layers. *Appl. Phys. Lett.* **2013**, *103*, 032402. [CrossRef]
7. Berger, L. Emission of spin waves by a magnetic multilayer traversed by a current. *Phys. Rev. B* **1996**, *54*, 9353. [CrossRef] [PubMed]
8. Diao, Z.; Li, Z.; Wang, S.; Ding, Y.; Panchula, A.; Chen, E.; Wang, L.-C.; Huai, Y. Spin-transfer torque switching in magnetic tunnel junctions and spin-transfer torque random access memory. *J. Phys. Condens. Matter* **2007**, *19*, 165209. [CrossRef]
9. Liu, H.; Bedau, D.; Backes, D.; Katine, J.; Langer, J.; Kent, A. Ultrafast switching in magnetic tunnel junction based orthogonal spin transfer devices. *Appl. Phys. Lett.* **2010**, *97*, 242510. [CrossRef]
10. Endoh, T.; Honjo, H.; Nishioka, K.; Ikeda, S. Recent progresses in STT-MRAM and SOT-MRAM for next generation MRAM. In Proceedings of the 2020 IEEE Symposium on VLSI Technology, Honolulu, HI, USA, 16–19 June 2020; pp. 1–2.
11. Ramazanov, S.; Sobola, D.; Orudzhev, F.; Knápek, A.; Polčák, J.; Potoček, M.; Kaspar, P.; Dallaev, R. Surface modification and enhancement of ferromagnetism in BiFeO3 nanofilms deposited on HOPG. *Nanomaterials* **2020**, *10*, 1990. [CrossRef]
12. Honjo, H.; Niwa, M.; Nishioka, K.; Nguyen, T.; Naganuma, H.; Endo, Y.; Yasuhira, M.; Ikeda, S.; Endoh, T. Influence of hard mask materials on the magnetic properties of perpendicular MTJs with double CoFeB/MgO interface. *IEEE Trans. Magn.* **2020**, *56*, 1–4. [CrossRef]
13. Pashen'kin, I.Y.; Sapozhnikov, M.; Gusev, N.S.; Rogov, V.; Tatarskii, D.A.; Fraerman, A.A.; Volochaev, M.N. Magnetoelectric effect in CoFeB/MgO/CoFeB magnetic tunnel junctions. *JETP Lett.* **2020**, *111*, 690–693. [CrossRef]
14. Jabeur, K.; Pendina, G.; Prenat, G. Study of spin transfer torque (STT) and spin orbit torque (SOT) magnetic tunnel junctions (MTJS) at advanced CMOS technology nodes. *Electr. Electron. Eng. Int. J.* **2017**, *6*, 1–9. [CrossRef]
15. Wolf, S.; Awschalom, D.; Buhrman, R.; Daughton, J.; von Molnár, V.S.; Roukes, M.; Chtchelkanova, A.Y.; Treger, D. Spintronics: A spin-based electronics vision for the future. *Science* **2001**, *294*, 1488–1495. [CrossRef]
16. Fert, A.; Van Dau, F.N. Spintronics, from giant magnetoresistance to magnetic skyrmions and topological insulators. *Comptes Rendus Phys.* **2019**, *20*, 817–831. [CrossRef]
17. Ota, S.; Ando, A.; Chiba, D. A flexible giant magnetoresistive device for sensing strain direction. *Nat. Electron.* **2018**, *1*, 124–129. [CrossRef]
18. Kubota, T.; Wen, Z.; Takanashi, K. Current-perpendicular-to-plane giant magnetoresistance effects using Heusler alloys. *J. Magn. Magn. Mater.* **2019**, *492*, 165667. [CrossRef]
19. Fujiwara, K.; Oogane, M.; Kanno, A.; Imada, M.; Jono, J.; Terauchi, T.; Okuno, T.; Aritomi, Y.; Morikawa, M.; Tsuchida, M.; et al. Magnetocardiography and magnetoencephalography measurements at room temperature using tunnel magneto-resistance sensors. *Appl. Phys. Express* **2018**, *11*, 023001. [CrossRef]
20. Liu, X.; Liu, C.; Han, W.; Pong, P.W. Design and implementation of a multi-purpose TMR sensor matrix for wireless electric vehicle charging. *IEEE Sens. J.* **2018**, *19*, 1683–1692. [CrossRef]
21. Paun, M.-A.; Sallese, J.-M.; Kayal, M. Hall effect sensors design, integration and behavior analysis. *J. Sens. Actuator Netw.* **2013**, *2*, 85–97. [CrossRef]
22. Zhu, T.; Chen, P.; Zhang, Q.; Yu, R.; Liu, B. Giant linear anomalous Hall effect in the perpendicular CoFeB thin films. *Appl. Phys. Lett.* **2014**, *104*, 202404. [CrossRef]
23. Ota, S.; Ono, M.; Matsumoto, H.; Ando, A.; Sekitani, T.; Kohno, R.; Iguchi, S.; Koyama, T.; Chiba, D. CoFeB/MgO-based magnetic tunnel junction directly formed on a flexible substrate. *Appl. Phys. Express* **2019**, *12*, 053001. [CrossRef]
24. Su, G.-Y.; You, M.-C.; Chuang, K.-W.; Wu, M.-H.; Hsieh, C.-H.; Lin, C.-Y.; Yang, C.-Y.; Anbalagan, A.K.; Lee, C.-H. Investigating Anisotropic Magnetoresistance in Epitaxially Strained CoFe Thin Films on a Flexible Mica. *Nanomaterials* **2023**, *13*, 3154. [CrossRef] [PubMed]
25. Xu, Z.; Qin, L. Effects of sputtering parameters and annealing temperatures on magnetic properties of CoFeB films. *J. Magn. Magn. Mater.* **2021**, *538*, 168302. [CrossRef]
26. Wang, K.; Alzate, J.; Amiri, P.K. Low-power non-volatile spintronic memory: STT-RAM and beyond. *J. Phys. D Appl. Phys.* **2013**, *46*, 074003. [CrossRef]
27. Julliere, M. Tunneling between ferromagnetic films. *Phys. Lett. A* **1975**, *54*, 225–226. [CrossRef]
28. Yuasa, S.; Nagahama, T.; Fukushima, A.; Suzuki, Y.; Ando, K. Giant room-temperature magnetoresistance in single-crystal Fe/MgO/Fe magnetic tunnel junctions. *Nat. Mater.* **2004**, *3*, 868–871. [CrossRef]

29. Yuasa, S.; Djayaprawira, D. Giant tunnel magnetoresistance in magnetic tunnel junctions with a crystalline MgO (0 0 1) barrier. *J. Phys. D Appl. Phys.* **2007**, *40*, R337. [CrossRef]
30. Tiusan, C.; Greullet, F.; Hehn, M.; Montaigne, F.; Andrieu, S.; Schuhl, A. Spin tunnelling phenomena in single-crystal magnetic tunnel junction systems. *J. Phys. Condens. Matter* **2007**, *19*, 165201. [CrossRef]
31. Ikeda, S.; Hayakawa, J.; Ashizawa, Y.; Lee, Y.; Miura, K.; Hasegawa, H.; Tsunoda, M.; Matsukura, F.; Ohno, H. Tunnel magnetoresistance of 604% at 300 K by suppression of Ta diffusion in CoFeB/MgO/CoFeB pseudo-spin-valves annealed at high temperature. *Appl. Phys. Lett.* **2008**, *93*, 082508. [CrossRef]
32. Liu, T.; Cai, J.; Sun, L. Large enhanced perpendicular magnetic anisotropy in CoFeB/MgO system with the typical Ta buffer replaced by an Hf layer. *Aip Adv.* **2012**, *2*, 032151. [CrossRef]
33. Lee, D.-Y.; Shim, T.-H.; Park, J.-G. Effects of Pt capping layer on perpendicular magnet anisotropy in pseudo-spin valves of Ta/CoFeB/MgO/CoFeB/Pt magnetic-tunneling junctions. *Appl. Phys. Lett.* **2013**, *102*, 212409. [CrossRef]
34. Shin, I.-J.; Min, B.-C.; Hong, J.P.; Shin, K.-H. Effects of Ru diffusion in exchange-biased MgO magnetic tunnel junctions prepared by in situ annealing. *Appl. Phys. Lett.* **2009**, *95*, 222501. [CrossRef]
35. Liu, T.; Zhang, Y.; Cai, J.; Pan, H. Thermally robust Mo/CoFeB/MgO trilayers with strong perpendicular magnetic anisotropy. *Sci. Rep.* **2014**, *4*, 5895. [CrossRef] [PubMed]
36. An, G.-G.; Lee, J.-B.; Yang, S.-M.; Kim, J.-H.; Chung, W.-S.; Hong, J.-P. Highly stable perpendicular magnetic anisotropies of CoFeB/MgO frames employing W buffer and capping layers. *Acta Mater.* **2015**, *87*, 259–265. [CrossRef]
37. Natarajarathinam, A.; Tadisina, Z.; Mewes, T.; Watts, S.; Chen, E.; Gupta, S. Influence of capping layers on CoFeB anisotropy and damping. *J. Appl. Phys.* **2012**, *112*, 053909. [CrossRef]
38. Takeuchi, Y.; Sato, H.; Fukami, S.; Matsukura, F.; Ohno, H. Temperature dependence of energy barrier in CoFeB-MgO magnetic tunnel junctions with perpendicular easy axis. *Appl. Phys. Lett.* **2015**, *107*, 152405. [CrossRef]
39. Enobio, E.C.I.; Bersweiler, M.; Sato, H.; Fukami, S.; Ohno, H. Evaluation of energy barrier of CoFeB/MgO magnetic tunnel junctions with perpendicular easy axis using retention time measurement. *Jpn. J. Appl. Phys.* **2018**, *57*, 04FN08. [CrossRef]
40. Park, C.; Kan, J.; Ching, C.; Ahn, J.; Xue, L.; Wang, R.; Kontos, A.; Liang, S.; Bangar, M.; Chen, H.; et al. Systematic optimization of 1 Gbit perpendicular magnetic tunnel junction arrays for 28 nm embedded STT-MRAM and beyond. In Proceedings of the 2015 IEEE International Electron Devices Meeting (IEDM), Washington, DC, USA, 7–9 December 2015; pp. 26.2.1–26.2.4.
41. Thomas, L.; Jan, G.; Le, S.; Lee, Y.-J.; Liu, H.; Zhu, J.; Serrano-Guisan, S.; Tong, R.-Y.; Pi, K.; Shen, D. Solving the paradox of the inconsistent size dependence of thermal stability at device and chip-level in perpendicular STT-MRAM. In Proceedings of the 2015 IEEE International Electron Devices Meeting (IEDM), Washington, DC, USA, 7–9 December 2015; pp. 26.4.1–26.4.4.
42. Bersweiler, M.; Sato, H.; Ohno, H. Magnetic and FREE-LAYER PROPERTIES of MgO/(Co) FeB/MgO structures: Dependence on CoFeB composition. *IEEE Magn. Lett.* **2017**, *8*, 1–3. [CrossRef]
43. Iwata-Harms, J.M.; Jan, G.; Liu, H.; Serrano-Guisan, S.; Zhu, J.; Thomas, L.; Tong, R.-Y.; Sundar, V.; Wang, P.-K. High-temperature thermal stability driven by magnetization dilution in CoFeB free layers for spin-transfer-torque magnetic random access memory. *Sci. Rep.* **2018**, *8*, 14409. [CrossRef]
44. Saito, T.; Ito, K.; Honjo, H.; Ikeda, S.; Endoh, T. Novel method of evaluating accurate thermal stability for MTJs using thermal disturbance and its demonstration for single-/double-interface p-MTJ. *IEEE Trans. Magn.* **2017**, *54*, 1–5. [CrossRef]
45. Igarashi, J.; Jinnai, B.; Desbuis, V.; Mangin, S.; Fukami, S.; Ohno, H. Temperature dependence of the energy barrier in X/1X nm shape-anisotropy magnetic tunnel junctions. *Appl. Phys. Lett.* **2021**, *118*, 012409. [CrossRef]
46. Meng, H.; Wang, J.-P. Spin transfer in nanomagnetic devices with perpendicular anisotropy. *Appl. Phys. Lett.* **2006**, *88*, 172506. [CrossRef]
47. Mangin, S.; Ravelosona, D.; Katine, J.; Carey, M.; Terris, B.; Fullerton, E.E. Current-induced magnetization reversal in nanopillars with perpendicular anisotropy. *Nat. Mater.* **2006**, *5*, 210–215. [CrossRef]
48. Liu, X.; Mazumdar, D.; Shen, W.; Schrag, B.; Xiao, G. Thermal stability of magnetic tunneling junctions with MgO barriers for high temperature spintronics. *Appl. Phys. Lett.* **2006**, *89*, 023504. [CrossRef]
49. Kishi, T.; Yoda, H.; Kai, T.; Nagase, T.; Kitagawa, E.; Yoshikawa, M.; Nishiyama, K.; Daibou, T.; Nagamine, M.; Amano, M.; et al. Lower-current and fast switching of a perpendicular TMR for high speed and high density spin-transfer-torque MRAM. In Proceedings of the 2008 IEEE International Electron Devices Meeting, San Francisco, CA, USA, 15–17 December 2008; pp. 1–4.
50. Wolf, S.A.; Lu, J.; Stan, M.R.; Chen, E.; Treger, D.M. The promise of nanomagnetics and spintronics for future logic and universal memory. *Proc. IEEE* **2010**, *98*, 2155–2168. [CrossRef]
51. Sato, H.; Yamanouchi, M.; Miura, K.; Ikeda, S.; Gan, H.; Mizunuma, K.; Koizumi, R.; Matsukura, F.; Ohno, H. Junction size effect on switching current and thermal stability in CoFeB/MgO perpendicular magnetic tunnel junctions. *Appl. Phys. Lett.* **2011**, *99*, 042501. [CrossRef]
52. Callen, E.; Callen, H. Ferromagnetic Transitions and the One-Third-Power Law. *J. Appl. Phys.* **1965**, *36*, 1140–1142. [CrossRef]
53. Jhajhria, D.; Pandya, D.K.; Chaudhary, S. Interplay of composition and anisotropy on evolution of microstructural, static and dynamic magnetic properties of CoFeB thin films on annealing. *J. Alloys Compd.* **2018**, *763*, 728–735. [CrossRef]
54. Franco, A. High temperature magnetic properties of cobalt ferrite nanoparticles. *Appl. Phys. Lett.* **2010**, *96*, 172505. [CrossRef]
55. Kim, S.; Baek, S.-H.C.; Ishibashi, M.; Yamada, K.; Taniguchi, T.; Okuno, T.; Kotani, Y.; Nakamura, T.; Kim, K.-J.; Moriyama, T.; et al. Contributions of Co and Fe orbitals to perpendicular magnetic anisotropy of MgO/CoFeB bilayers with Ta, W, IrMn, and Ti underlayers. *Appl. Phys. Express* **2017**, *10*, 073006. [CrossRef]

56. Ishibe, T.; Maeda, Y.; Terada, T.; Naruse, N.; Mera, Y.; Kobayashi, E.; Nakamura, Y. Resistive switching memory performance in oxide hetero-nanocrystals with well-controlled interfaces. *Sci. Technol. Adv. Mater.* **2020**, *21*, 195–204. [CrossRef]
57. Tu, W.-T.; Wang, C.-H.; Huang, Y.-Y.; Lin, W.-C. Growth and magnetism of low-temperature deposited Fe/Si (111) films as an intermediate layer for suppression of silicide formation. *J. Appl. Phys.* **2011**, *109*, 023908. [CrossRef]
58. Iwata-Harms, J.M.; Jan, G.; Serrano-Guisan, S.; Thomas, L.; Liu, H.; Zhu, J.; Lee, Y.-J.; Le, S.; Tong, R.-Y.; Patel, S.; et al. Ultrathin perpendicular magnetic anisotropy CoFeB free layers for highly efficient, high speed writing in spin-transfer-torque magnetic random access memory. *Sci. Rep.* **2019**, *9*, 19407. [CrossRef]
59. Park, E.-S.; Lee, D.-K.; Xue, F.; Min, B.-C.; Koo, H.C.; Haney, P.M.; Kim, K.-W.; Lee, K.-J. Strong higher-order angular dependence of spin-orbit torque in W/CoFeB bilayer. *Phys. Rev. B* **2023**, *107*, 064411. [CrossRef]
60. Kalarickal, S.S.; Krivosik, P.; Wu, M.; Patton, C.E.; Schneider, M.L.; Kabos, P.; Silva, T.J.; Nibarger, J.P. Ferromagnetic resonance linewidth in metallic thin films: Comparison of measurement methods. *J. Appl. Phys.* **2006**, *99*, 093909. [CrossRef]
61. Lu, G.; Huang, X.; Fan, S.; Ling, W.; Liu, M.; Li, J.; Jin, L.; Pan, L. Temperature-and thickness-dependent dynamic magnetic properties of sputtered CoFeB/Ta bilayer films. *J. Alloys Compd.* **2018**, *753*, 475–482. [CrossRef]
62. Haidar, M.; Ranjbar, M.; Balinsky, M.; Dumas, R.; Khartsev, S.; Åkerman, J. Thickness-and temperature-dependent magnetodynamic properties of yttrium iron garnet thin films. *J. Appl. Phys.* **2015**, *117*, 17D119. [CrossRef]
63. Maier-Flaig, H.; Klingler, S.; Dubs, C.; Surzhenko, O.; Gross, R.; Weiler, M.; Huebl, H.; Goennenwein, S.T. Temperature-dependent magnetic damping of yttrium iron garnet spheres. *Phys. Rev. B* **2017**, *95*, 214423. [CrossRef]
64. Kittel, C. On the theory of ferromagnetic resonance absorption. *Phys. Rev.* **1948**, *73*, 155. [CrossRef]
65. Kamberský, V. Spin-orbital Gilbert damping in common magnetic metals. *Phys. Rev. B* **2007**, *76*, 134416. [CrossRef]
66. Sakuma, A. First-principles study on the Gilbert damping constants of transition metal alloys, Fe–Ni and Fe–Pt systems. *J. Phys. Soc. Jpn.* **2012**, *81*, 084701. [CrossRef]
67. Takeuchi, Y.; Enobio, E.C.I.; Jinnai, B.; Sato, H.; Fukami, S.; Ohno, H. Temperature dependence of intrinsic critical current in perpendicular easy axis CoFeB/MgO magnetic tunnel junctions. *Appl. Phys. Lett.* **2021**, *119*, 242403. [CrossRef]
68. Malinowski, G.; Kuiper, K.; Lavrijsen, R.; Swagten, H.; Koopmans, B. Magnetization dynamics and Gilbert damping in ultrathin Co48Fe32B20 films with out-of-plane anisotropy. *Appl. Phys. Lett.* **2009**, *94*, 102501. [CrossRef]
69. Deorani, P.; Yang, H. Role of spin mixing conductance in spin pumping: Enhancement of spin pumping efficiency in Ta/Cu/Py structures. *Appl. Phys. Lett.* **2013**, *103*, 232408. [CrossRef]
70. He, C.; Navabi, A.; Shao, Q.; Yu, G.; Wu, D.; Zhu, W.; Zheng, C.; Li, X.; He, Q.L.; Razavi, S.A. Spin-torque ferromagnetic resonance measurements utilizing spin Hall magnetoresistance in W/Co40Fe40B20/MgO structures. *Appl. Phys. Lett.* **2016**, *109*, 202404. [CrossRef]
71. Diaz, J.; Hamdan, N.; Jalil, P.; Hussain, Z.; Valvidares, S.; Alameda, J. Understanding the magnetic anisotropy in Fe-Si amorphous alloys. *IEEE Trans. Magn.* **2002**, *38*, 2811–2813. [CrossRef]
72. Ajan, A.; Abarra, E.; Acharya, B.; Inomata, A.; Okamoto, I.; Shinohara, M. Thermal effects and in-plane magnetic anisotropy in thin-film recording media. *Appl. Phys. Lett.* **2003**, *82*, 1075–1077. [CrossRef]
73. Sharrock, M. Time dependence of switching fields in magnetic recording media. *J. Appl. Phys.* **1994**, *76*, 6413–6418. [CrossRef]